# Oscillating spin Hall effect from polaron transport in organic chains

G. C. Hu,[1,*] Y. Y. Miao,[1] and C. Timm[2,3,†]

[1]*School of Physics and Electronics, Shandong Normal University, Jinan 250358, China*

[2]*Institute of Theoretical Physics, Technische Universität Dresden, 01062 Dresden, Germany*

[3]*Würzburg-Dresden Cluster of Excellence ct.qmat, Technische Universität Dresden, 01062 Dresden, Germany*

(Received 30 June 2022; revised 15 September 2022; accepted 12 October 2022; published 21 October 2022)

The polaron dynamics in organic ladders is calculated in the presence of electron-lattice and spin-orbit couplings (SOCs), employing an extended Su-Schrieffer-Heeger (SSH) model and a nonadiabatic dynamics method. The time-dependent total charge and spin in the chains is averaged over initial polaron states with spins up and down. This average reveals a strong oscillating spin Hall effect (SHE). We show the necessity of all terms in the SSH Hamiltonian for the SHE, including intrachain and interchain hopping as well as intrachain and interchain SOC. The large and rapidly oscillating behavior of the SHE is verified to originate from the existence of polarons by comparison with the case of rigid chains without polarons. We attribute the enhancement of the SHE to skew scattering off transient deformations of the chains. Spectral analysis exhibits three dominant parts in the Fourier-transformed spin Hall signal. The high-frequency part is associated with the pure spin-flip dynamics due to SOC, while the low-frequency parts, which are also observed in the charge response, are related to the intrinsic electron transfer between the chains and the appearance of polarons, respectively. In this paper, we reveal the distinct properties of the dynamical SHE in organics dominated by polaron transport.

DOI: 10.1103/PhysRevB.106.144309

## I. INTRODUCTION

The spin Hall effect (SHE) [1–5] and its Onsager inverse, the inverse SHE (ISHE) [6–9], realize the conversion between orthogonal charge and spin currents. These effects are of high current interest in the field of spintronics. They have been widely investigated for inorganic metals [6,7,10] and semiconductors [8,11,12] with large atomic numbers since efficient spin-orbit (SO) interaction is usually necessary for a sizable intrinsic SHE [4]. Organic spintronics is an emerging field exploring the application of the electron spin in organic molecules [13–15], which allows one to fabricate flexible, large-area, and low-cost electronic devices by chemical techniques. Although the realization of the SHE in organics is highly desirable, it is challenged because the atomic SO coupling (SOC) in organics is weak due to the small atomic numbers of the constituent atoms. Clearly, stronger SOC is expected in the presence of heavier atoms. Intriguingly, recent experimental and theoretical investigations have revealed that the effective strength of SOC can also be sizable in the presence of structural modulation. For example, it has been confirmed that, when atoms from the third or higher period of the periodic table are contained in the molecule, such as Al in tris-(8-hydroxyquinoline) aluminum ($Alq_3$) and Cu in copper phthalocyanine (CuPc), the SOC has a significant effect on the spin relaxation [16,17]. Topological-insulator states and the quantum anomalous Hall effect were also predicted in two-dimensional (2D) organic-metal grids [18,19]. Authors of many experimental and theoretical works have demonstrated the dependence of the SOC strength on molecular structure and chemical components [20,21], where the value can be increased by nearly four orders of magnitude via structural modulation [22,23]. These studies suggest that the SHE is feasible in organics.

In experiments, the ISHE in poly(3,4-ethylenedioxythiophene) (PEDOT) organic molecules doped by poly(4-styrenesulphonate) (PSS) was reported by Ando *et al.* [24]. A high spin-charge-conversion efficiency comparable with platinum was proposed, and it was deduced that the long spin lifetime and large conductivity anisotropy of the organic material are crucial. Sun *et al.* [25] further measured the ISHE in organic semiconductors with different SOC strengths. However, the ISHE in PEDOT-PSS was questioned by Wang *et al.* [26], who claimed that the spin-charge conversion phenomenon resulted from the Seebeck effect caused by the temperature gradient rather than from the ISHE. The ISHE in highly doped PEDOT-PSS was subsequently quantified by Qaid *et al.* [27]. On the theoretical side, using the master-equation method, Yu *et al.* [28] calculated the SHE due to hopping conducting in a highly disordered organic solid. First-principles methods were applied to determine the SOC parameters and to calculate the spin Hall conductivity [29,30].

Despite the experimental progress for the ISHE in organics, the issue remains open because of a lack of understanding of the microscopic processes. Pioneering theoretical works [28,30] were limited to the extension of the picture of spin-charge conversion via electron transport in inorganic materials to organics. They thus did not fully consider the unique structural properties of organic materials, such as the strong electron-lattice (e-l) coupling and the resulting polarons composed of charge, spin, and lattice distortions. Authors of

*hgc@sdnu.edu.cn

†carsten.timm@tu-dresden.de

 

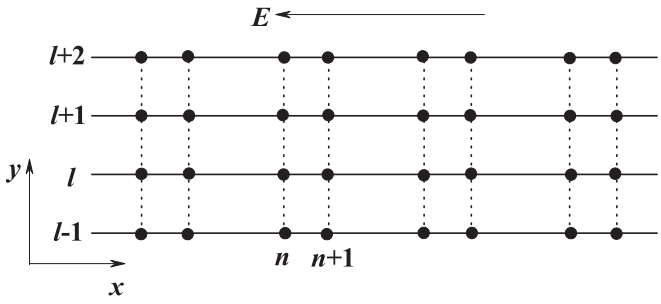


FIG. 1. Schematic of the organic lattice.

experimental studies have indicated the importance of polarons for the transport of spin [31]. Thus, more theoretical support concerning the microscopic mechanism of the SHE in organics is required, considering the unique characteristics of organics.

In this paper, we construct quasi-one-dimensional ladder models for organic thin films and investigate the polaron dynamics in the presence of SOC, on the basis of the extended Su-Schrieffer-Heeger (SSH) model [32]. Similar models have also been applied in the research on topological phases and topological edge states [33,34]. In this paper, by considering the SOC and tracing the charge and spin evolution, a picture of the SHE via polaron transport is revealed. The remainder of the paper is organized as follows: In Sec. II, the model and the calculation method are introduced. In Sec. III, the numerical calculations for the polaron dynamics are performed, and the results are discussed. A brief summary is given in Sec. IV.

## II. MODEL AND METHODS

As shown in Fig. 1, we consider an organic lattice composed of several weakly coupled $\pi$-conjugated polymer chains, reflecting the fact that, in most organic films, the intrachain coupling is strong, while the interchain coupling is much weaker. The system can be described by the extended SSH model considering the interchain coupling and the SOC, where the Hamiltonian is given by [32,35]

$$H = H_e + H_{\text{latt}}. \tag{1}$$

Here, $H_e = H_0 + H_{\text{so}}$ is the Hamiltonian of the $\pi$ electrons, where $H_0$ describes the electron hopping in the framework of the tight-binding model:

$$\begin{aligned} H_0 = &-\sum_{l,n,\sigma} t^l_{n,n+1}(c^\dagger_{l,n+1,\sigma}c_{l,n,\sigma} + \text{H.c.}) \\ &- t^\perp \sum_{l,n,\sigma}(c^\dagger_{l+1,n,\sigma}c_{l,n,\sigma} + \text{H.c.}). \end{aligned} \tag{2}$$

Here, $t^l_{n,n+1}$ is the intrachain hopping integral between sites $n$ and $n+1$ of chain $l$, which is expanded in terms of the lattice distortion as $t^l_{n,n+1} = t_0 - \alpha(u_{l,n+1} - u_{l,n})$, where $t_0$ denotes the hopping integral between two neighboring sites in a uniform chain, $\alpha$ is the e-l coupling constant, and $u_{l,n}$ is the displacement of site $n$ in chain $l$ from its equilibrium position along the $x$ direction. The e-l coupling allows for the Peierls dimerization expected for the one-dimensional chains [36,37].

Here, $c^\dagger_{l,n,\sigma}$ ($c_{l,n,\sigma}$) is the electron creation (annihilation) operator for site $(l, n)$ with spin $\sigma$. $t^\perp$ is the longitudinal interchain hopping integral between chains $l$ and $l+1$, which for simplicity is assumed to be uniform and unchanged regardless of the displacement $u_{l,n}$.

Here, $H_{\text{so}}$ is the Hamiltonian describing the SO interaction. Here, we use a tight-binding model for the Rashba effect, which reads as [35]

$$\begin{aligned} H_{\text{so}} = &-t_{\text{so}} \sum_{l,n,\sigma,\sigma'} [c^\dagger_{l,n+1,\sigma'}(i\sigma_y)_{\sigma'\sigma}c_{l,n,\sigma} + \text{H.c.}] \\ &+ t^\perp_{\text{so}} \sum_{l,n,\sigma,\sigma'} [c^\dagger_{l+1,n,\sigma'}(i\sigma_x)_{\sigma'\sigma}c_{l,n,\sigma} + \text{H.c.}], \end{aligned} \tag{3}$$

where $t_{\text{so}}$ and $t^\perp_{\text{so}}$ are the intrachain and interchain SO-interaction strengths, respectively, and $\sigma_x$ and $\sigma_y$ are Pauli matrices.

Here, $H_{\text{latt}}$ is the lattice part of the total Hamiltonian, which is described classically as

$$H_{\text{latt}} = \frac{M}{2}\sum_{l,n}\dot{u}^2_{l,n} + \frac{K}{2}\sum_{l,n}(u_{l,n+1} - u_{l,n})^2, \tag{4}$$

where $M$ is the mass, and $K$ is the elastic constant.

As initial state for the dynamics simulations, the eigenstate $|\Psi_\mu\rangle$ with eigenenergy $\varepsilon_\mu$ of the organic lattice can be obtained by solving the electronic Schrödinger equation:

$$H_e|\Psi_\mu\rangle = \varepsilon_\mu|\Psi_\mu\rangle, \tag{5}$$

where $\mu$ is the label of the eigenstate. The eigenstate is expanded in Wannier space as $|\Psi_\mu\rangle = \sum_{l,n,\sigma}\psi^\mu_{l,n,\sigma}|l, n, \sigma\rangle$, where $\psi^\mu_{l,n,\sigma}$ is the wave function at site $(l, n)$ for spin $\sigma$. Thus, the electronic Schrödinger equation turns into

$$\begin{aligned} \varepsilon_\mu\psi^\mu_{l,n,\sigma} = &-t^l_{n-1,n}\psi^\mu_{l,n-1,\sigma} - t^l_{n,n+1}\psi^\mu_{l,n+1,\sigma} \\ &- t^\perp\psi^\mu_{l-1,n,\sigma} - t^\perp\psi^\mu_{l+1,n,\sigma} \\ &- t_{\text{so}}\big(\psi^\mu_{l,n-1,\uparrow}\delta_{\sigma,\downarrow} - \psi^\mu_{l,n-1,\downarrow}\delta_{\sigma,\uparrow} \\ &\quad + \psi^\mu_{l,n+1,\downarrow}\delta_{\sigma,\uparrow} - \psi^\mu_{l,n+1,\uparrow}\delta_{\sigma,\downarrow}\big) \\ &+ it^\perp_{\text{so}}\big(\psi^\mu_{l-1,n,\uparrow}\delta_{\sigma,\downarrow} + \psi^\mu_{l-1,n,\downarrow}\delta_{\sigma,\uparrow} \\ &\quad - \psi^\mu_{l+1,n,\downarrow}\delta_{\sigma,\uparrow} - \psi^\mu_{l+1,n,\uparrow}\delta_{\sigma,\downarrow}\big), \end{aligned} \tag{6}$$

where $\delta_{\sigma,\uparrow(\downarrow)}$ equals 1 for $\sigma = \uparrow$ ($\downarrow$) and zero otherwise. After solving the electronic Schrödinger equation, the lattice distortion is obtained by minimizing the total energy of the system by solving $\partial E[\{u_{l,n}\}]/\partial u_{l,n} = 0$, which leads to the equation:

$$u_{l,n+1} - u_{l,n} = -\frac{2\alpha}{K}\,\text{Re}\,\rho^l_{n,n+1} + \frac{2\alpha}{NK}\sum_{n'=1}^{N}\text{Re}\,\rho^l_{n',n'+1}, \tag{7}$$

where $N$ is the total number of sites in each chain, and the last term results from the constraint of fixed total length. The charge density matrix $\rho^l$ is defined by its components $\rho^l_{n,n'} = \rho^l_{n,n',\uparrow} + \rho^l_{n,n',\downarrow}$, with

$$\rho^l_{n,n',\sigma} = \sum_\mu \psi^{\mu*}_{l,n,\sigma} f_{\mu,\sigma}\psi^\mu_{l,n',\sigma}, \tag{8}$$

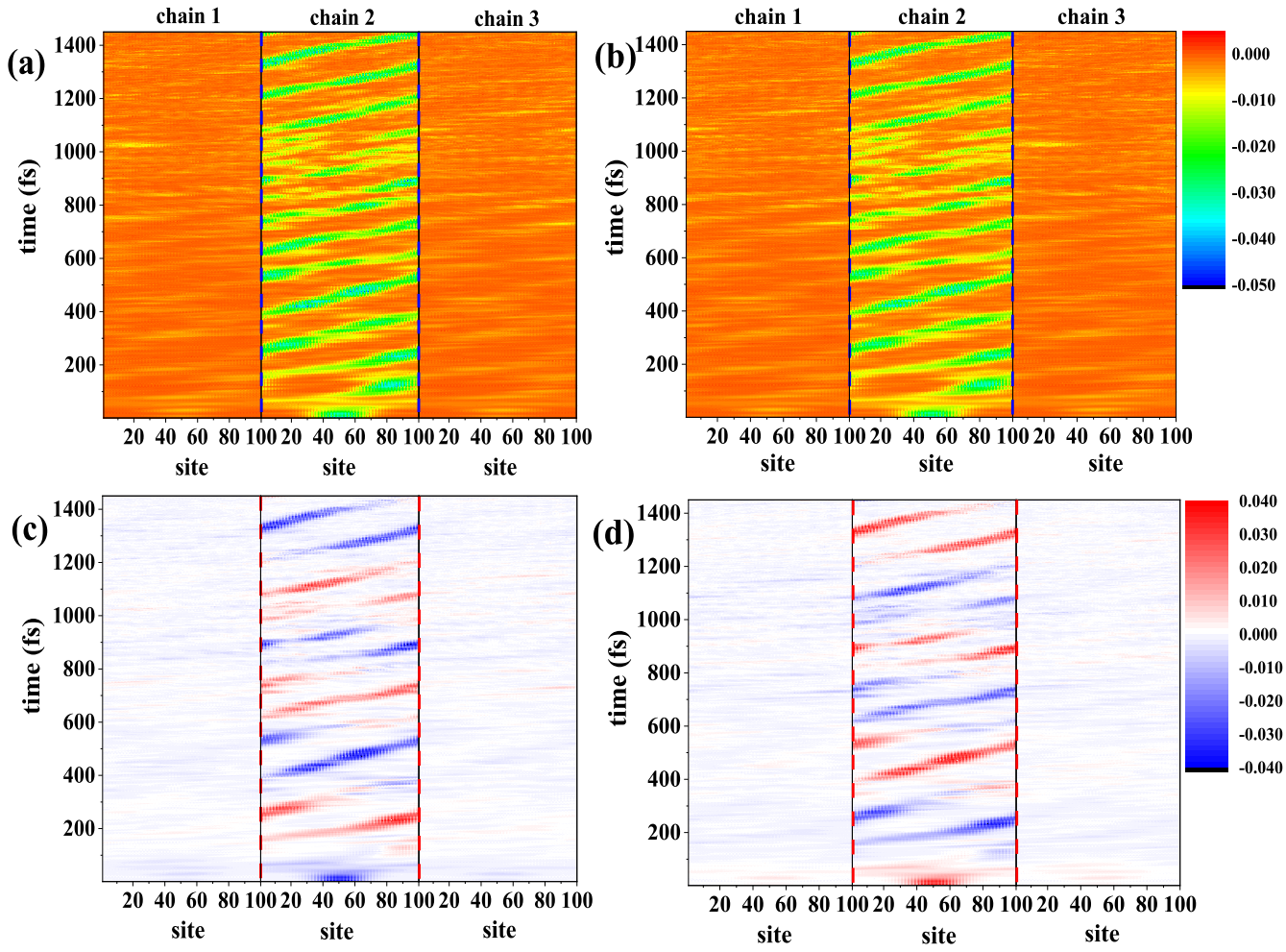


FIG. 2. Time evolution of the charge (in units of $e$) and spin (in units of $\hbar/2$) for a polaron initially localized on the middle chain. Charge density for the (a) spin-down and (b) spin-up polarons. Spin density for the (c) spin-down and (d) spin-up polarons.

where $f_{\mu,\sigma}$ is the distribution function determined by the initial occupation, which is 0 or 1. Periodic boundary conditions are adopted for the $x$ direction along the chain to facilitate a long time evolution for the polaron dynamics. Open boundary conditions are used for the $y$ direction. Equations (6) and (7) need to be solved self-consistently.

In the presence of an electric field of strength $E$ along the negative $x$ direction, the electronic Hamiltonian is modified as

$$H_0(t) = -\sum_{l,n,\sigma} t^l_{n,n+1}\,[\exp(-i\gamma A)c^\dagger_{l,n+1,\sigma}c_{l,n,\sigma} + \text{H.c.}] - t^\perp \sum_{l,n,\sigma}(c^\dagger_{l+1,n,\sigma}c_{l,n,\sigma} + \text{H.c.}), \tag{9}$$

$$H_{\text{so}}(t) = -t_{\text{so}} \sum_{l,n,\sigma,\sigma'} [\exp(-i\gamma A)c^\dagger_{l,n+1,\sigma'}(i\sigma_y)_{\sigma'\sigma}c_{l,n,\sigma} + \text{H.c.}] + t^\perp_{\text{so}} \sum_{l,n,\sigma,\sigma'} [c^\dagger_{l+1,n,\sigma'}(i\sigma_x)_{\sigma'\sigma}c_{l,n,\sigma} + \text{H.c.}]. \tag{10}$$

The exponential term is generated by the electric field in the case of periodic boundary conditions [38,39]. Here, the coefficient $\gamma$ is defined as $ea/\hbar$, with $e$ and $a$ being the elementary charge and the lattice constant of each chain, respectively. The electric field is given by $E(t) = -\partial_t A(t)$ [38]. The time evolution of the electronic states is described by the time-dependent Schrödinger equation:

$$\begin{aligned} i\hbar\frac{\partial}{\partial t}\psi^\mu_{l,n,\sigma} = &-t^l_{n-1,n}\exp(-i\gamma A)\psi^\mu_{l,n-1,\sigma} - t^l_{n,n+1}\exp(i\gamma A)\psi^\mu_{l,n+1,\sigma} - t^\perp\psi^\mu_{l-1,n,\sigma} - t^\perp\psi^\mu_{l+1,n,\sigma} \\ &- t_{\text{so}}\big[\exp(-i\gamma A)\psi^\mu_{l,n-1,\uparrow}\delta_{\sigma,\downarrow} - \exp(-i\gamma A)\psi^\mu_{l,n-1,\downarrow}\delta_{\sigma,\uparrow} \\ &+ \exp(i\gamma A)\psi^\mu_{l,n+1,\downarrow}\delta_{\sigma,\uparrow} - \exp(i\gamma A)\psi^\mu_{l,n+1,\uparrow}\delta_{\sigma,\downarrow}\big] \\ &+ it^\perp_{\text{so}}\big[\psi^\mu_{l-1,n,\uparrow}\delta_{\sigma,\downarrow} + \psi^\mu_{l-1,n,\downarrow}\delta_{\sigma,\uparrow} - \psi^\mu_{l+1,n,\downarrow}\delta_{\sigma,\uparrow} - \psi^\mu_{l+1,n,\uparrow}\delta_{\sigma,\downarrow}\big]. \end{aligned} \tag{11}$$

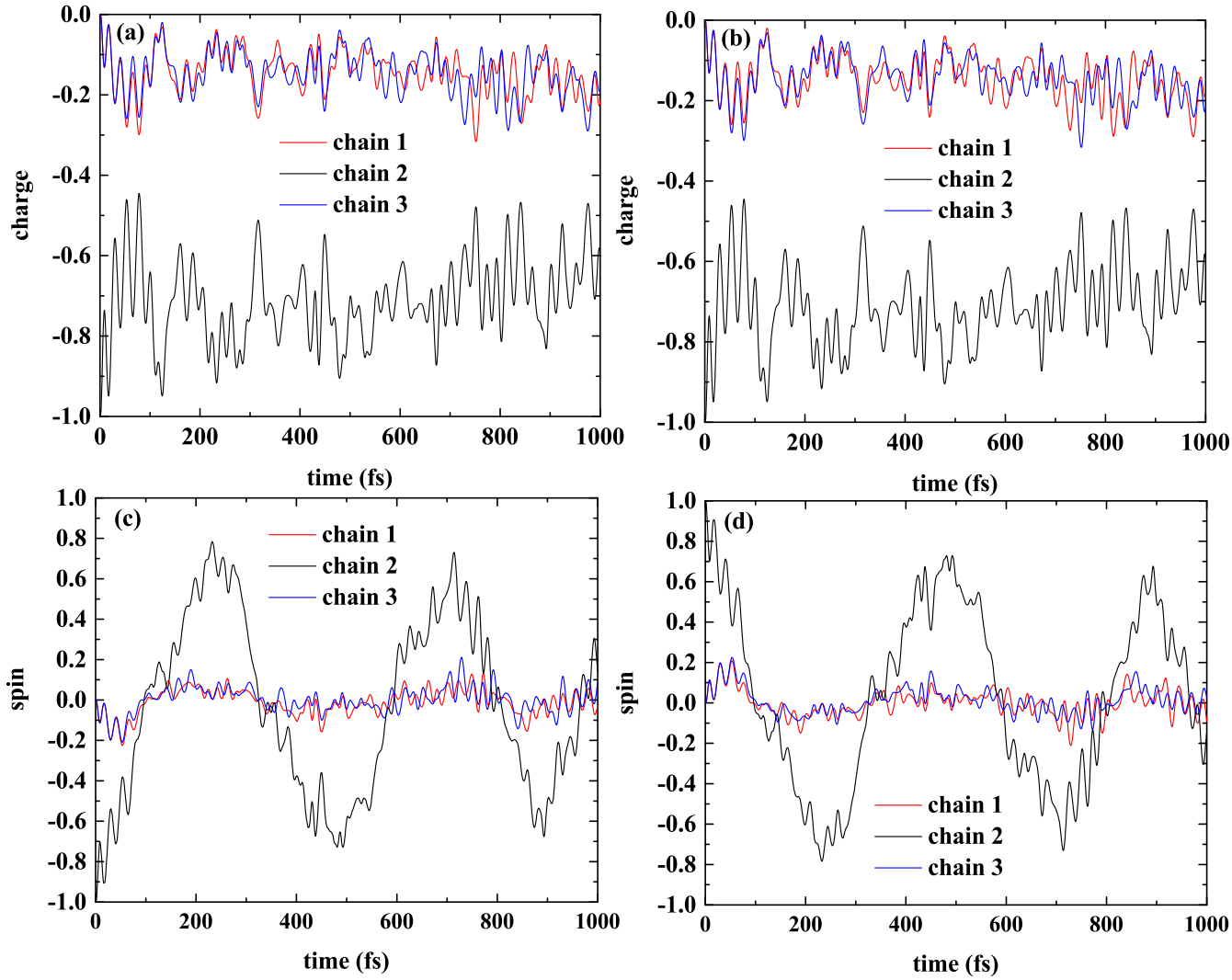


FIG. 3. Time evolution of the total charge (in units of $e$) and total spin (in units of $\hbar/2$) in each of the chains for a polaron initially localized on the middle chain. Charge density for the (a) spin-down and (b) spin-up polarons. Spin density for the (c) spin-down and (d) spin-up polarons.

Within our half-classical treatment, the lattice distortion is determined by Newton's equation of motion:

$$M\ddot{u}_{l,n}(t) = 2\alpha \mathrm{Re}\big[\exp(i\gamma A)\big(\rho^{l}_{n,n+1} - \rho^{l}_{n-1,n}\big)\big] - K\,(2u_{l,n} - u_{l,n+1} - u_{l,n-1}). \tag{12}$$

The two coupled differential Eqs. (11) and (12) can be resolved numerically with a Runge-Kutta method of order eight with step-size control [40], which has been used widely and successfully to describe polaron dynamics [41,42]. After obtaining the time-dependent wave function, the charge density and the $z$ component of the spin density at each site are defined as

$$Q_{l,n}(t) = 1 - \rho^{l}_{n,n}(t), \tag{13}$$

$$S^{z}_{l,n}(t) = \frac{\hbar}{2}\big[\rho^{l}_{n,n,\uparrow}(t) - \rho^{l}_{n,n,\downarrow}(t)\big]. \tag{14}$$

For the numerical calculations, parameters are chosen as describing *trans*-polyacetylene [37], $t_0 = 2.5\,\mathrm{eV}$, $\alpha = 4.1\,\mathrm{eV/\AA}$, $K = 21.0\,\mathrm{eV/\AA^2}$, $a = 1.22\,\mathrm{\AA}$, and $M = 1349.14\,\mathrm{eV\,fs^2\,\AA^{-2}}$. The results are expected to apply qualitatively to other conjugated polymers as well. A small interchain hopping integral $t^{\perp} = 0.05\,\mathrm{eV}$ is used. For simplicity, the SOC is assumed to be $t_{\mathrm{so}} = 2t^{\perp}_{\mathrm{so}} = 0.02\,\mathrm{eV}$. Comparable values of the SOC parameters have been used in Ref. [39]. Since the interchain-coupling and SOC parameters depend on the morphology and can thus be tuned, for example, by strain, effects of their strength will be further discussed in the following. The maximum of the electric field is set to $E_0 = 3 \times 10^{-4}\,\mathrm{V/\AA}$. The field is ramped up linearly with time as $E(t) = E_0 t/t_c$ for $0 < t < t_c$ and $E(t) = E_0$ for $t \geqslant t_c$. Here, $t_c = 30\,\mathrm{fs}$ is the turn-on time.

## III. RESULTS AND DISCUSSION

### A. Oscillating SHE in organic chains

We first consider three coupled chains with $N = 100$ sites for each chain. As the initial state, a fully spin-polarized polaron is assumed to be located in the center of the middle

chain (around the sites 30–70 in chain 2). To be specific, we take the lowest-energy polaronic eigenstates of a single chain. In nonmagnetic conjugated polymers, there exist degenerate spin-up and spin-down polarons. Hence, both kinds of polarons are considered in our calculations, realized by introducing an extra electron occupying the degenerate lowest unoccupied molecular orbital (LUMO) with spin up or spin down. The dynamics is different in these two cases due to the SOC.

In Fig. 2, the time evolution of the charge and spin densities for each kind of polaron are plotted. We can see that the polaron remains mainly localized on the middle chain and follows an obvious trajectory, moving against the field with approximately constant velocity. The charge distribution on the middle chain is the same for the spin-down polaron, Fig. 2(a), and the spin-up polaron, Fig. 2(b), for all times. Small parts of the charge and spin diffuse into the upper and lower chains (chains 1 and 3) due to the weak interchain couplings $t^{\perp}$ and $t_{so}^{\perp}$. Spin precession of the polaron is clearly visible in Figs. 2(c) and 2(d), for both the spin-up and the spin-down polaron, especially for chain 2. The spin precession of the polaron during transport along the chains is caused by the intrachain SOC $t_{so}$, as has been well demonstrated in previous works [39,43].

To get a quantitative view on the evolution of charge and spin in different directions, we calculate the time-dependent total charge and total spin in each chain. The results are shown in Fig. 3. For the spin-down polaron, the total charges in each chain oscillate with time due to charge transfer between the chains. The maximum transferred charges into chains 1 and 3 are $\sim 0.3\,e$. The spins in each chain precess with the same period of $\sim$400 fs, which is much longer than the timescale of the charge transfer between the chains. The spin magnitude changes from $\sim -0.8$ to 0.8 for chain 2 and $-0.2$ to 0.2 for chains 1 and 3. Despite the different values of the total spin in each chain, the precession period is the same due to the identical intrachain SOC strength.

Due to symmetry, the evolution of the polaron charges is the same for the spin-up polaron and the spin-down polaron except that the charges in chains 1 and 3 are interchanged. Moreover, the total spins in all chains are inverted, and the spins in chains 1 and 3 are interchanged.

In nonmagnetic polymers in vanishing magnetic field, spin-up and spin-down polarons are energetically degenerate. Therefore, we assume that the spin-up and spin-down polarons contribute equally to the transport. We can then investigate the charge and spin evolution of the system within an statistical average over the two kinds of polarons. This average describes an unpolarized current flowing through the chain, which is the typical situation in SHE experiments [11]. In Fig. 4, we plot the averaged total charge and total spin in each chain as functions of time, which are simply calculated by summing these quantities for the two kinds of polarons and dividing by 2. It is clearly seen that the averaged charges in chains 1 and 3 are identical at all times, which means that there is no net charge displacement in the $y$ direction, and only a charge current along the $x$ direction is induced by the electric field. The averaged total spins shown in Fig. 4(b) demonstrate that the net spin in chain 2 always remains zero, whereas the spin is nonzero in chains 1 and 3, with the same magnitude

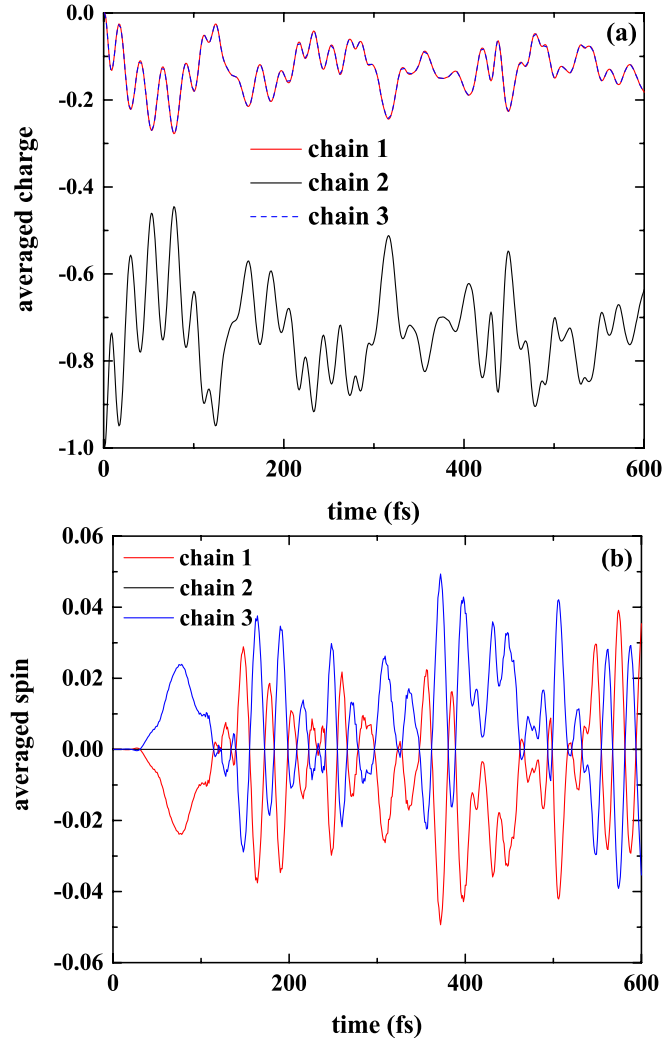


FIG. 4. (a) Total charges and (b) total spins in each chain as functions of time, averaged over spin-down and spin-up polarons.

and opposite signs in all times. The averaged total spins in the two edge chains oscillate irregularly with time. We have simulated the dynamics up to 6000 fs with different parameters (not shown), where these oscillations are still observed in the presence of polarons. From the above, it can be concluded that, in the present system, an oscillating pure spin current along the $y$ direction is generated by a pure charge current along the $x$ direction. In other words, there is an oscillating SHE.

Next, we analyze the mechanism of the oscillating SHE. First, the necessity of each parameter for this effect is examined. The intrachain hopping $t_{n,n+1}^{l}$ is necessary for the presence of polarons. Here, we numerically examine the roles of the parameters $t^{\perp}$, $t_{so}$, and $t_{so}^{\perp}$ as well as of the field $E$. Each of these quantities is set as zero individually, and the polaron dynamics is simulated. Figure 5 shows the evolution of spins in chains 1 and 3 in the case of the spin-down polaron. It is found that, if any one of $t^{\perp}$, $t_{so}$, $t_{so}^{\perp}$, or $E$ is set to zero, the spins in the two chains are identical at all times. The same happens for an spin-up polaron (not shown). After statistical averaging over the two spin directions, the spins in all chains

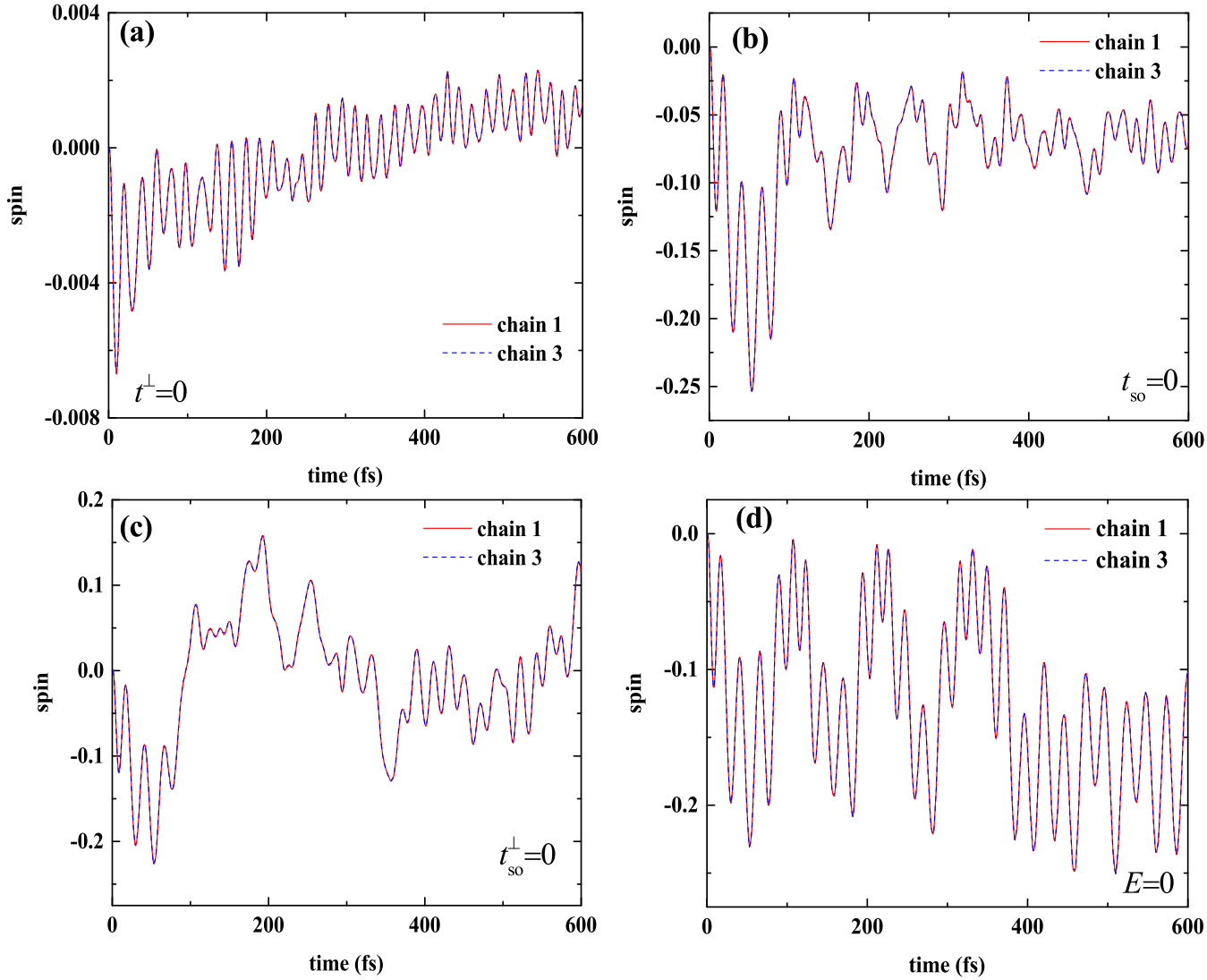


FIG. 5. Total spins in chains 1 and 3 as functions of time, averaged over spin-down and spin-up polarons, for (a) $t^{\perp} = 0$, (b) $t_{so} = 0$, (c) $t^{\perp}_{so} = 0$, and (d) $E = 0$. In each case, the nonzero parameters are the same as in Fig. 2.

stay zero, and the SHE vanishes. We thus find that all of the above parameters are essential for the SHE.

The necessity of the various coupling terms for the SHE can be understood as follows. The observable of interest is the total spin polarization along the $z$ direction in chain $l$, i.e.,

$$S_{z,l} = \sum_{n,\sigma,\sigma'} c^{\dagger}_{l,n,\sigma'} \frac{(\sigma_z)_{\sigma'\sigma}}{2} c_{l,n,\sigma}. \tag{15}$$

The initial state is an equal mixture of a spin-up polaron and a spin-down polaron in the central chain. We can describe this state by the statistical operator:

$$\rho(t=0) = \tfrac{1}{2}\,|\uparrow\rangle\langle\uparrow| + \tfrac{1}{2}\,|\downarrow\rangle\langle\downarrow|, \tag{16}$$

where $|\uparrow\rangle$ ($|\downarrow\rangle$) is the state containing a spin-up (spin-down) polaron. In spin space, $\rho(0)$ is proportional to the unit matrix and hence is SU(2) invariant under global spin rotations. Therefore, the spin polarization at the initial time $\langle S_{z,l}\rangle(0) = \mathrm{Tr}\,\rho(0)S_{z,l}$ vanishes. The time-dependent spin polarization is $\langle S_{z,l}\rangle(t) = \mathrm{Tr}\,\rho(t)S_{z,l}$. The essential point is that, whenever any one of the parameters $t^{\perp}$, $t_{so}$, $t^{\perp}_{so}$, or $t^{l}_{n,n+1}$ is zero, that is, whenever one term in the Hamiltonian $H_e(t) = H_0(t) + H_{so}(t)$ in Eqs. (9) and (10) vanishes, the system possesses a U(1) symmetry. For example, in the case of $t_{so} = 0$, $H_e(t)$ will only contain the single Pauli matrix $\sigma_x$, and thus, it is U(1) invariant under spin rotation about the $x$ axis. Since the initial state $\rho(0)$ has the same invariance, the time evolution generated by $H_e(t)$ can only lead to $\rho(t)$ that retains this U(1) symmetry. Hence, only a spin polarization along the $x$ axis is allowed so that $\langle S_{z,l}\rangle(t) = 0$. The arguments for the cases when $t^{\perp}_{so}$, $t^{\perp}$, or $t^{l}_{n,n+1}$ are zero are analogous, as shown in the Appendix.

The necessity of a nonzero electric field $E$ seen in Fig. 5(d) has a different origin. For $E = 0$, the system is symmetric under time reversal, and no spin polarization can be generated out of the unpolarized initial state.

The above analysis shows that all coupling terms in our model are required for the SHE. The oscillating behavior of the SHE remains to be clarified. Note that an oscillating SHE was also proposed for a strongly localized 2D electron gas

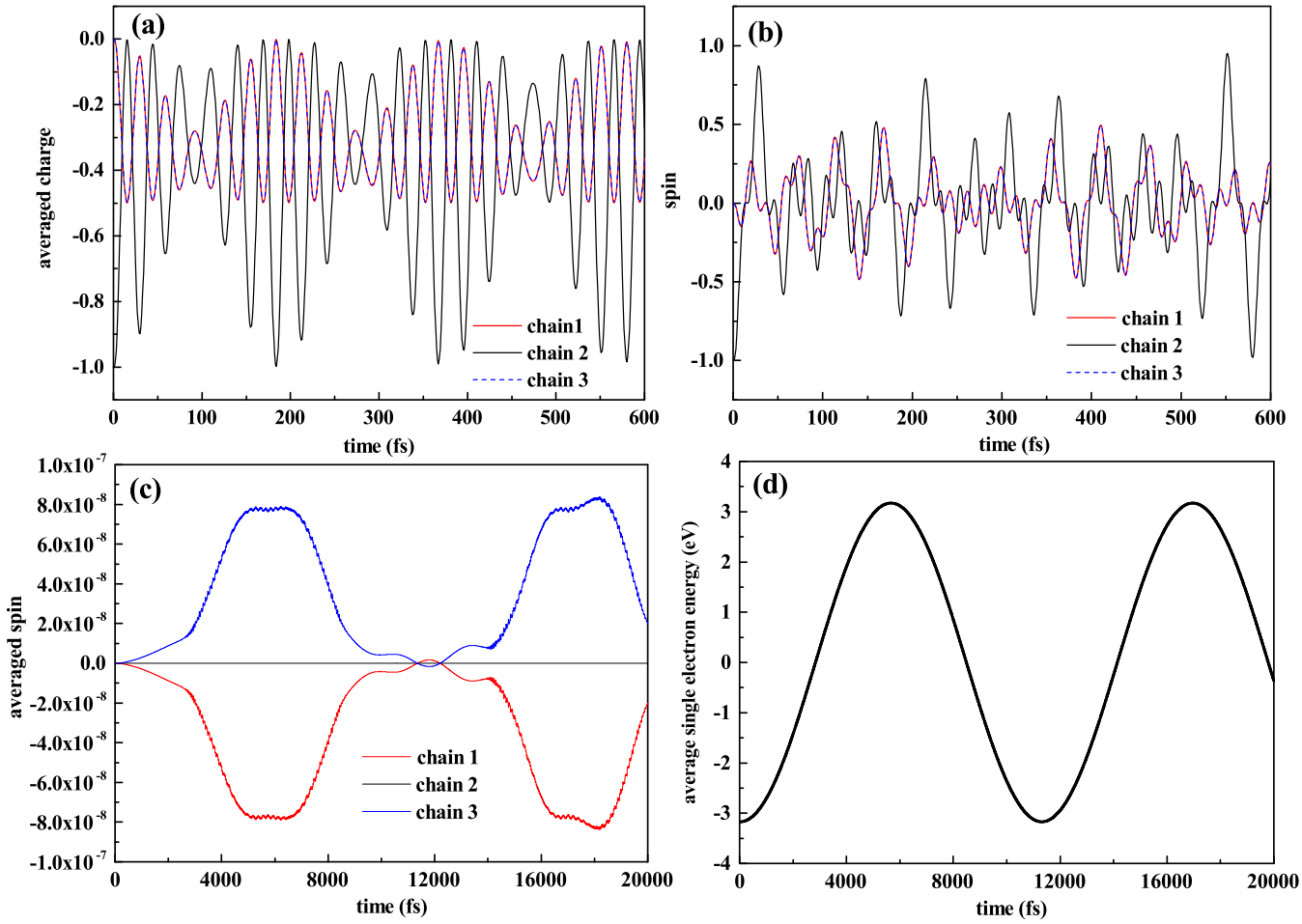


FIG. 6. (a) Total charges and (c) total spins in each chain as functions of time, averaged over spin-down and spin-up initial states, for uniform rigid chains without polarons. (b) Total spins in each chain for the spin-down polaron. (d) Average single-electron energy as a function of time. The parameters are the same as in Fig. 2, except for $\alpha = 0$. Note the tiny numerical scale of the averaged spins in (c).

with Rashba SO interaction and electron-phonon coupling [44]. However, an oscillating electric field is required in this scenario. In contrast, we predict an oscillating SHE for a static electric field.

The rapidly oscillating SHE with large amplitude can be traced back to the characteristics of organic materials, specifically to the polaron formation. To show this, we have performed calculations for the charge and spin evolution for three uniform rigid chains with $\alpha = 0$. In this case, the extra electron occupies a delocalized Bloch state (the LUMO of the half-filled chain) rather than a wave-packet-like polaron state. As shown in Fig. 6, time-dependent oscillations are observed for the averaged total charges, like organic chains. Both the amplitude and frequency for chains 1 and 3 are enlarged compared with the organic model. However, although the total spin in chains 1 and 3 is large and oscillating, the spin averaged over the two spin directions of the initial state is much smaller, by a factor on the order of $10^{-6}$, compared with Fig. 4(b) [45]. The results imply that, with the same strength of the SOC, the charge-spin conversion is much more efficient for polaron transport than for bare Bloch electrons.

Moreover, the oscillations of the averaged total spin shown in Fig. 6(c) are much slower than for the organic model. The observed period on the order of 12 000 fs corresponds to the Bloch oscillation of the extra electron. The Bloch oscillation period is clearly reflected in Fig. 6(d), where the average single-electron energy at each time is calculated from the total electron energy divided by the electron number.

How can one understand the numerical observation that polaron formation is essential for the large and rapidly oscillating SHE in organic chains? From the point of view of the fast electronic hopping processes, the lattice deformation is quasistatic and thus acts as a scattering potential for the electrons. This scattering does not involve SOC in our model since it results from the inhomogeneity of the intrachain hopping $t^l_{n,n+1}$. The scattering of electrons with intrinsic SOC by non-SO disorder generically leads to two contributions to the SHE: skew scattering and intrinsic side-jump scattering [5]. One difference between these two mechanisms is that the skew-scattering contribution is proportional to the transport lifetime $\tau$ of the electrons, whereas the side-jump contribution is independent of $\tau$. We will see in Sec. III B that the SHE decreases for increasing e-l coupling $\alpha$. Larger $\alpha$ enhances the scattering and thus reduces $\tau$. Hence, the SHE decreases for decreasing $\tau$, which is consistent with dominant skew scattering but not side-jump scattering. We conclude that the rigid chains only show a weak intrinsic SHE, whereas the large SHE in organic chains is dominated by skew scattering. As

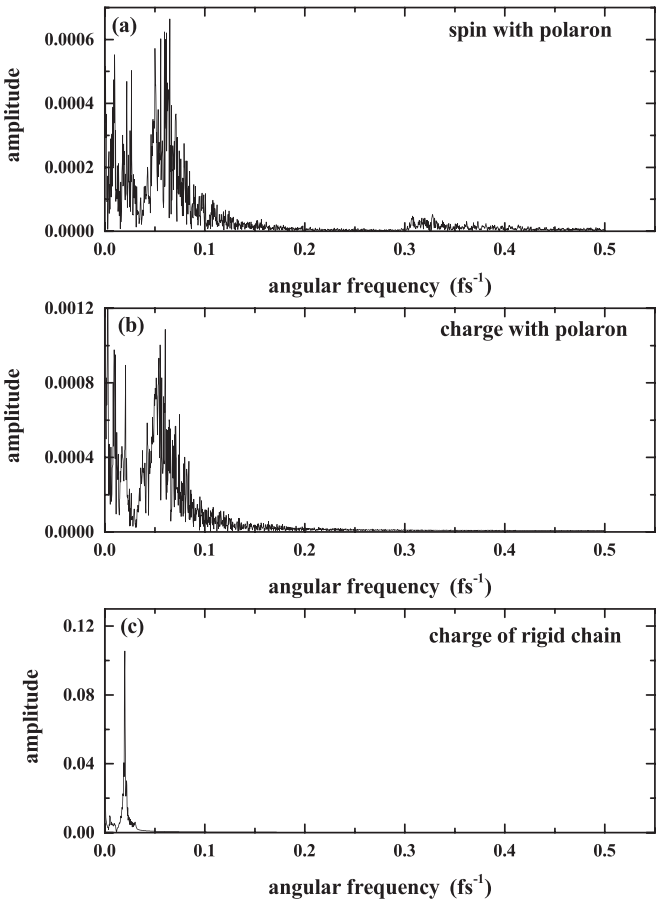


FIG. 7. Fast Fourier transform (FFT) of the time evolution of (a) averaged total spin and (b) averaged total charge in chain 1 in the presence of polarons. Here, $t^{\perp} = 0.03\,\mathrm{eV}$, and the other parameters are the same as in Fig. 2. (c) FFT of the averaged total charges in the case of uniform rigid chains without polarons ($\alpha = 0$).

for the rapid oscillations, these are also present in the charge transfer between the chains for the rigid case, see Fig. 6(a), but hardly visible in the SHE, Fig. 6(c). Enabling a strong SHE by skew scattering makes these oscillations visible in the SHE.

Our results are consistent with measurement by Ando *et al.* [24], where the spin-charge conversion efficiency in PEDOT : PSS was found to be comparable with platinum, although the SOC strength in organics is about four orders of magnitude weaker than in platinum.

### B. Fourier analysis

Since the oscillations of the spins and charges shown in Figs. 2–6 are complicated, we have performed a spectral analysis to find contributions with characteristic frequency scales. In Fig. 7(a), we plot the fast Fourier transform (FFT) of the averaged total spin in chain 1. The spectrum shows three characteristic frequency ranges, two low-frequency parts at angular frequencies $\sim$0.02 and $0.06\,\mathrm{fs}^{-1}$ and a broad high-frequency part from 0.3 to $0.5\,\mathrm{fs}^{-1}$. The amplitude of the two low-frequency parts is much larger than the one of the high-frequency part.

In the present system, the oscillations of the spins in the upper and lower chains can be attributed to three mechanisms: One is the slow oscillation of the electrons between the three chains, which can also be seen in the charge, both for organic chains and for uniform rigid chains, cf. Figs. 7(b) and 7(c). Another is the appearance of the polaron due to the e-l interaction, which implies that the spins are carried by localized states and hence modifies the spin evolution. The last is the spin-flip spin transfer between the chains caused by SOC. To confirm this picture, we plot the FFT for the averaged charges in chain 1 in the presence of the polaron in Fig. 7(b). It is found that the high-frequency part vanishes, which means that it is contributed by the pure spin dynamics from the SOC. In Fig. 7(c), we further plot the FFT for the averaged total charges for the case of uniform rigid chains without polaron formation. It is seen that the second low-frequency part $\sim 0.06\,\mathrm{fs}^{-1}$ is absent. This shows that the appearance of the polarons not only contributes to the high-frequency spin dynamics but also changes the low-frequency oscillations of the charges.

We have also investigated the effects of the various model parameters on the magnitude and oscillation frequency of the SHE. In the following, the interchain coupling $t^{\perp}$, the SOCs $t_{\mathrm{so}}$ and $t_{\mathrm{so}}^{\perp}$, and the e-l interaction $\alpha$ are considered, which are common variables relying on the species and morphology of organic materials. Figure 8 shows the time-dependent averaged total spins in each chain and the corresponding FFT for chain 1 at $t^{\perp} = 0.02$ and 0.04 eV. It is found that the magnitude of the oscillating SHE at 0.04 eV is about twice that at 0.02 eV. From the FFT, the amplitudes of the two low-frequency parts are strongly enhanced by $t^{\perp}$, while the high-frequency part is hardly affected. This is because $t^{\perp}$ promotes both the charge and the spin transfer between chains but is unrelated to the spin-flip spin transfer.

The effect of the SOC strength is shown in Fig. 9. Obviously, the magnitude of the SHE is increased by $t_{\mathrm{so}}$ and $t_{\mathrm{so}}^{\perp}$. The FFT shows that the high-frequency part gains weight rapidly with the increase of the SOC strength. This is consistent with the above observation that the high-frequency part is due to spin-flip dynamics. Moreover, the two low-frequency parts are also enhanced and merge into a broad peak, which reflects the fact that the interchain SOC also contributes to charge transfer.

The dependence of the SHE on the e-l interaction strength $\alpha$ is shown in Fig. 10. Increasing $\alpha$ reduces the magnitude of the SHE. The FFT analysis shows the decrease of amplitudes for all three parts, accompanied by a large shift of the high-frequency part to a higher onset frequency and a smaller shift of the low-frequency part $\sim 0.06\,\mathrm{fs}^{-1}$. This is because a larger $\alpha$ induces a stronger lattice distortion as well as a larger polaron effective mass [46]. We suggest that the accompanying enhancement of the polaron localization impedes the transfer of both charge and spin between chains.

### C. SHE in five chains

Finally, we have simulated the polaron dynamics for a larger system with five organic chains. Each chain consists of 100 sites, as above. The polaron is initially localized on the middle chain (chain 3). The total spins averaged over the two spin orientations of the initial polaron state are calculated with the same parameters as in Fig. 2 and are shown in Fig. 11. An oscillating SHE is still observed in this case, where the

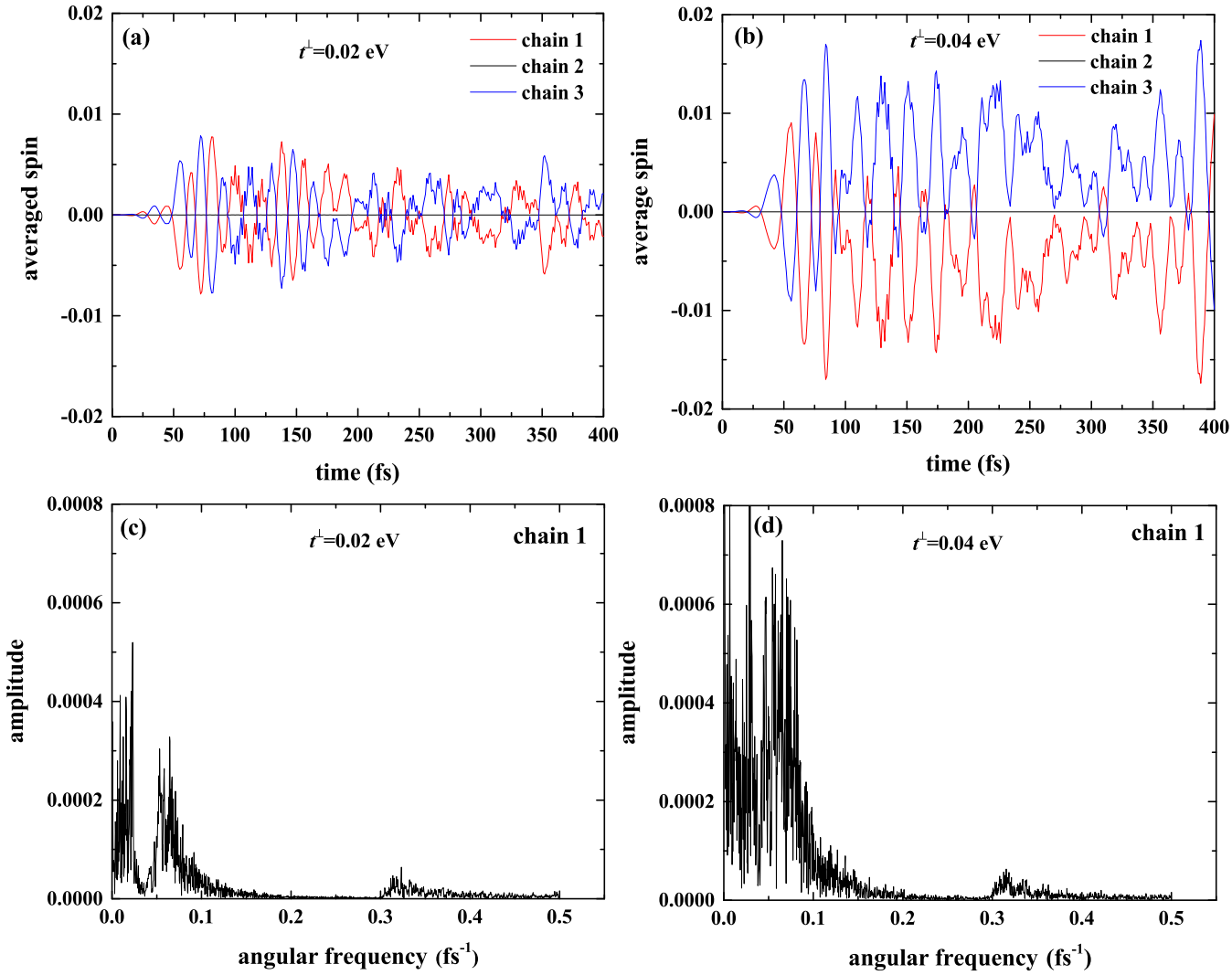


FIG. 8. Averaged total spins in each chain for (a) $t^{\perp} = 0.02$ eV and (b) $t^{\perp} = 0.04$ eV. (c) and (d) Corresponding fast Fourier transform (FFT) of the time evolution of the averaged spins in chain 1. The other parameters are the same as in Figs. 7(a) and 7(b).

oscillating amplitude in the two intermediate chains (2 and 4) is initially larger than the one in the two edge chains (1 and 5), and later the amplitudes become comparable. The maximum magnitude of the SHE at times up to 600 fs is ∼0.09, which is roughly twice the value for the three-chain system shown in Fig. 4. This suggests that the oscillating SHE is not limited to narrow ladders but rather can be observed in large systems.

## IV. SUMMARY AND CONCLUSIONS

We have investigated the polaron dynamics for coupled organic chains in the presence of intrachain and interchain SOC. By analyzing the time-dependent charge and spin in each chain, averaged over the two possible spin states of the polaron, an oscillating SHE is found: An oscillating spin current in the transverse direction is generated by a longitudinal charge current. Theoretical analysis proves that all coupling terms in the present model, i.e., the intrachain hopping $t^{l}_{n,n+1}$, the interchain coupling $t^{\perp}$, the intrachain SOC $t_{\rm so}$, and the interchain SOC $t^{\perp}_{\rm so}$, are necessary for the SHE. In the absence of any one of them, the system satisfies a U(1) spin-rotation symmetry, which prevents the separation of spins in the transverse direction.

The large, oscillating SHE is revealed to be caused by the presence of polarons by comparison with the case of delocalized Bloch electrons on uniform rigid chains. While this comparison yields clear numerical evidence, it does not provide a physical explanation. Based on the observation that larger e-l coupling, which leads to stronger scattering of the electrons off the quasistatic lattice deformations and thus, to a smaller electron transport time, reduces the SHE, we argue that the enhancement of the SHE is due to skew scattering of the electrons. A spectral analysis performed by Fourier transformation of the oscillating spin and charge demonstrates that there exist three separate frequency ranges in the response. The high-frequency part is contributed by pure spin-flip dynamics between the chains due to the SOC. The two low-frequency parts, which are also observed in the charge degree of freedom, are related to the intrinsic electron transfer between the chains and the appearance of polarons, respectively.

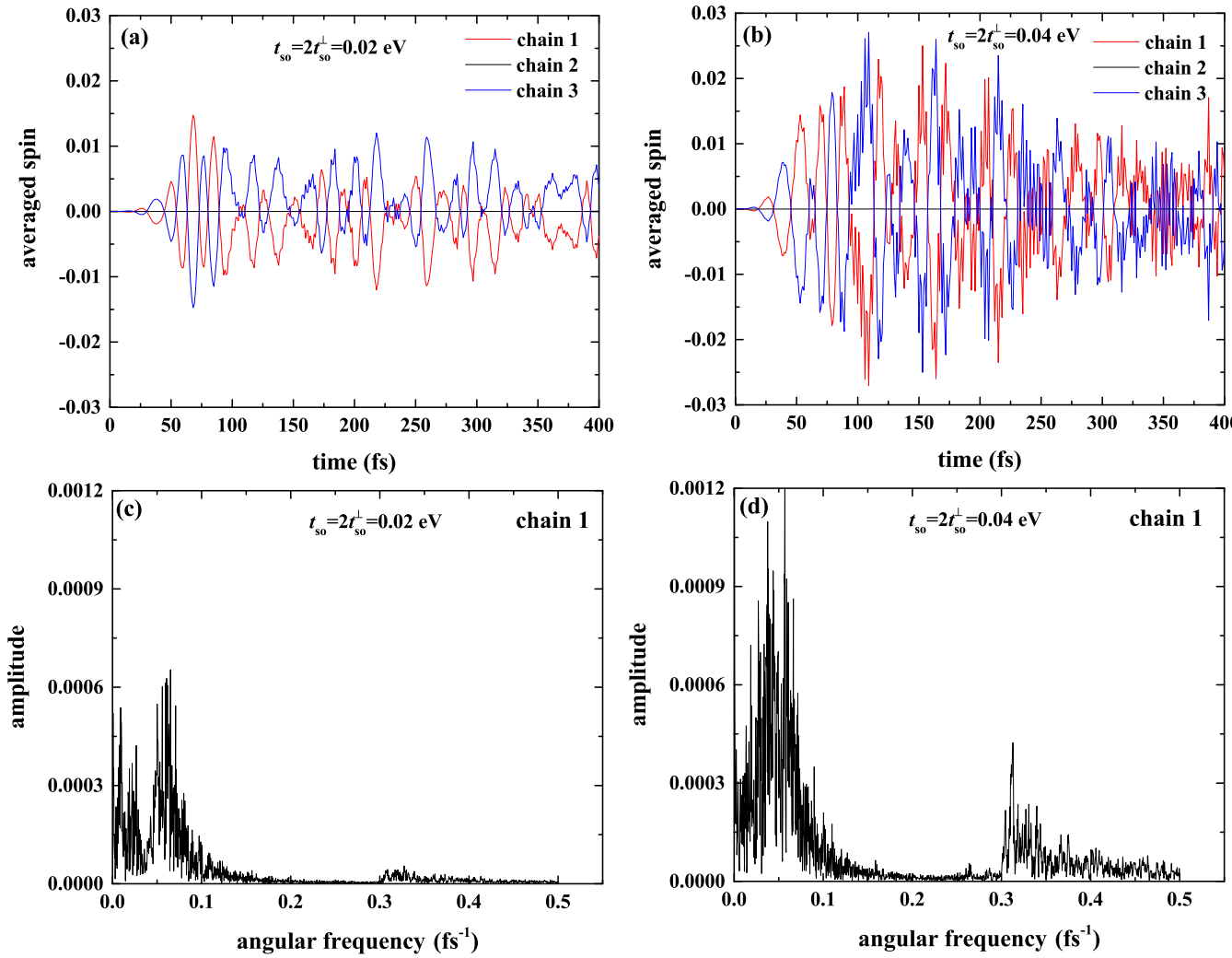


FIG. 9. Averaged total spins in each chain for (a) $t_{so} = 2t_{so}^{\perp} = 0.02$ eV and (b) $t_{so} = 2t_{so}^{\perp} = 0.04$ eV. (c) and (d) Corresponding fast Fourier transform (FFT) of the time evolution of the averaged spins in chain 1. The other parameters are the same as in Figs. 7(a) and 7(b).

The oscillating SHE is also seen for five coupled organic chains and is comparable in magnitude with the case of three chains. It should be mentioned that, although only results for odd numbers of chains are displayed in this paper since these systems allow a symmetric polaron position in the $y$ direction and thus facilitate the interpretation of the results in terms of the SHE, the proposed phenomenon also occurs for even numbers of chains. We have performed numerical simulations for two chains with an initial interchain polaron and also observe the oscillating SHE.

Furthermore, in real polymers, the electron-electron interaction is inevitable. We have checked that, in the framework of the Hubbard model treated in mean-field approximation, the oscillating SHE is robust in the presence of electron-electron interaction, except for a slight modification of the amplitude and frequency.

All the above results indicate that the proposed phenomenon will be measurable in experiments. The SHE does not decrease from 3 to 5 chains. This gives hope that it is also sizable in the 2D limit. Checking this conjecture is a promising direction for future theoretical research. Note that our results are directly applicable to 2D layers of electrically isolated three-leg and five-leg ladders: The spins in the bulk of the system compensate each other on average, but at the edges, there is nothing to compensate them, and a nonzero edge polarization survives. Hence, one should observe the SHE at the edges. In experiments, one could use magneto-optical Kerr microscopy to measure the spin accumulation at the transverse edges, as demonstrated for inorganic materials [11]. In summary, in this paper, we predict a large, oscillating SHE in organic materials dominated by polaron transport and exhibit its characteristics, which are expected to be tested by future experiments.

## ACKNOWLEDGMENTS

Support from the National Natural Science Foundation of China (Grant No. 11974215) and the Natural Science Foundation of Shandong Province (No. ZR2019MA043) are gratefully acknowledged. C.T. gratefully acknowledges support by the Deutsche Forschungsgemeinschaft via the Collaborative Research Center SFB 1143, Project No. A04, and the Cluster of Excellence on Complexity and Topology in Quantum Matter ct.qmat (EXC 2147, Project ID 390858490).

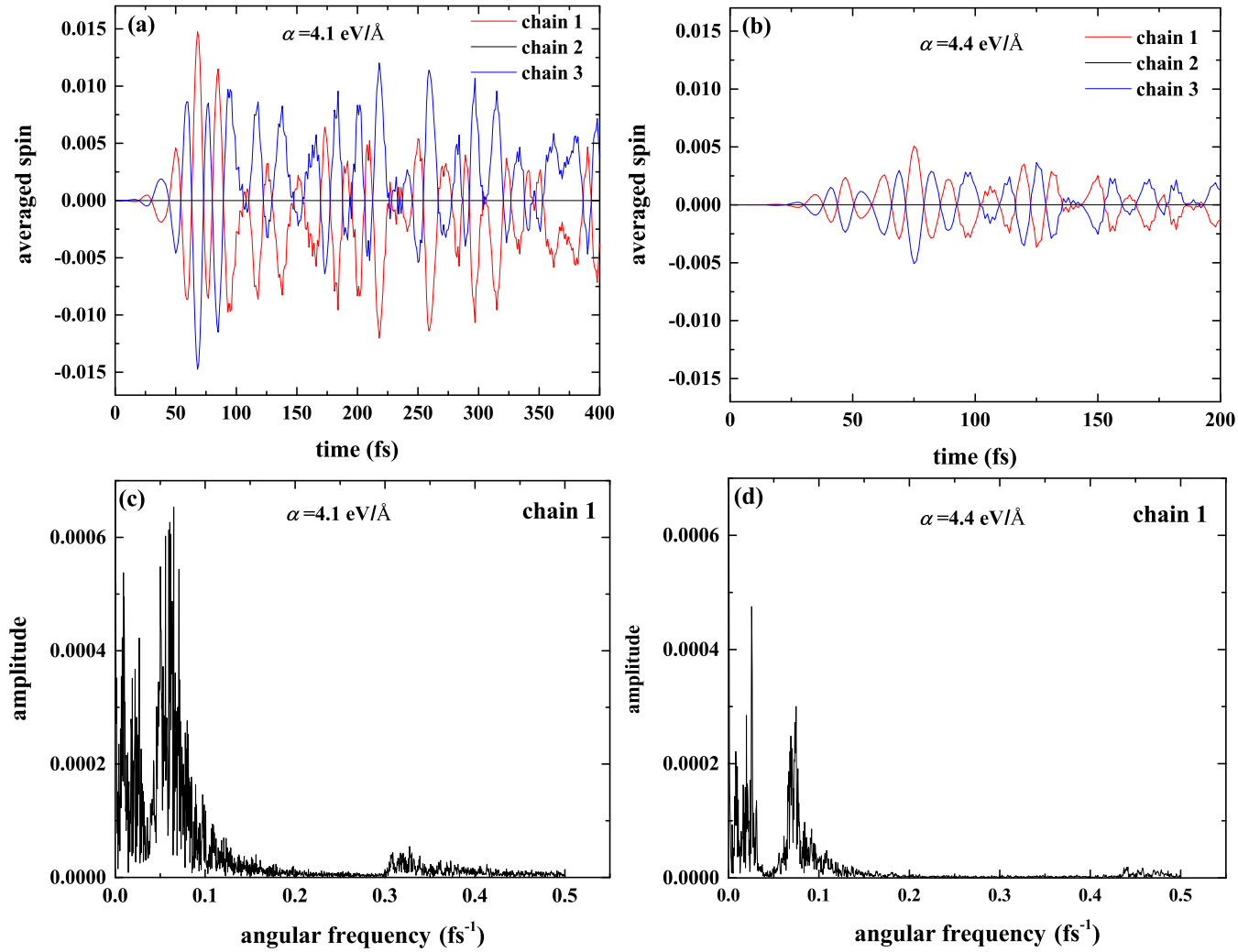


FIG. 10. Averaged total spins in each chain for (a) $\alpha = 4.1\,\mathrm{eV/Å}$ and (b) $\alpha = 4.4\,\mathrm{eV/Å}$. (c) and (d) Corresponding fast Fourier transform (FFT) of the time evolution of the averaged spins in chain 1. The other parameters are the same as in Figs. 7(a) and 7(b).

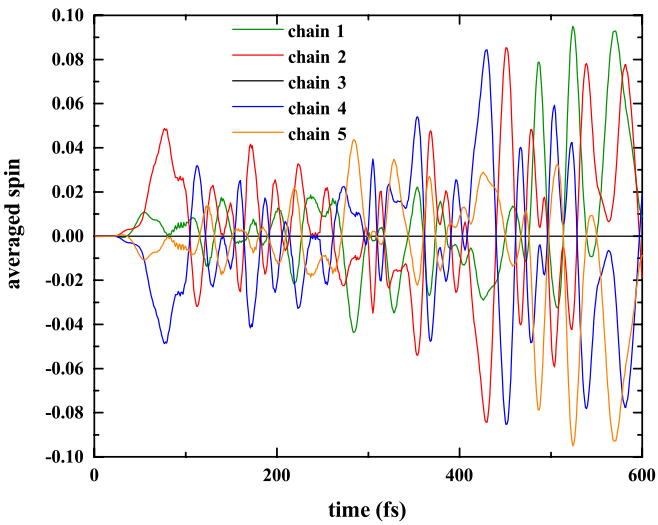


FIG. 11. (a) Total charges and (b) total spins in each chain as functions of time, averaged over spin-down and spin-up polarons, for a model with five organic chains. The parameters are the same as in Fig. 2.

## APPENDIX A: NECESSITY OF ALL TERMS IN THE HAMILTONIAN

In this Appendix, we show that all four terms in the electronic Hamiltonian $H_e = H_0 + H_{\mathrm{so}}$ are required to obtain the SHE. The observable of interest is the total spin polarization in the $z$ direction in chain $l$, i.e.,

$$S_{z,l} = \sum_n c^\dagger_{l,n} \frac{\sigma_z}{2} c_{l,n}, \tag{A1}$$

where $c_{l,n}$ is a spinor operator. We show that $\langle S_{z,l}\rangle(t) = \mathrm{Tr}\,\rho(t)\,S_{z,l}$ stays zero for all times whenever (at least) one of the terms in the Hamiltonian $H$ vanishes. The proof will rely on the presence of a U(1) symmetry whenever one of the terms is zero.

*Case 1*: $t_{\mathrm{so}} = 0$. Since $H_e$ only contains the single Pauli matrix $\sigma_x$, it is U(1) invariant under spin rotation about the $x$ axis. Since the initial state $\rho(0) = (1/2)(|\uparrow\rangle\langle\uparrow| + |\downarrow\rangle\langle\downarrow|)$ has the same invariance, the time evolution generated by $H_e$ can only lead to $\rho(t)$ that retain this U(1) symmetry. Hence, only a spin polarization along the $x$ axis is allowed, and $\langle S_{z,l}\rangle(t) = 0$.

*Case 2*: $t^{\perp}_{\rm so} = 0$. Since $H_e$ only contains the Pauli matrix $\sigma_y$, it is U(1) invariant under spin rotation about the $y$ axis. The argument is analogous to the previous case.

*Case 3*: $t^{l}_{n,n+1} = 0$. To exhibit the U(1) invariance, we introduce new fermionic operators:

$$d_{l,n} = (-i\sigma_y)^n\, c_{l,n}, \qquad d^{\dagger}_{l,n} = c^{\dagger}_{l,n}\,(i\sigma_y)^n, \tag{A2}$$

from which

$$c_{l,n} = (i\sigma_y)^n\, d_{l,n}, \qquad c^{\dagger}_{l,n} = d^{\dagger}_{l,n}\,(-i\sigma_y)^n. \tag{A3}$$

The Hamiltonian then reads as

$$\begin{aligned} H = &-t^{\perp}\sum_{l,n}(d^{\dagger}_{l+1,n}d_{l,n} + \text{H.c.}) \\ &+t_{\rm so}\sum_{l,n}[\exp(-i\gamma A)d^{\dagger}_{l,n+1}d_{l,n} + \text{H.c.}] \\ &+t^{\perp}_{\rm so}\sum_{l,n}(-1)^n\,(d^{\dagger}_{l+1,n}i\sigma_x d_{l,n} + \text{H.c.}). \end{aligned} \tag{A4}$$

The transformed Hamiltonian only contains the Pauli matrix $\sigma_x$ and thus is U(1) invariant under rotations of the spin of the new fermions about the $x$ axis.

We also must show that the initial state is invariant under rotations of this new spin. To this end, we calculate the average of this spin at an arbitrary site $(l, n)$ in the initial state:

$$\begin{aligned} &\langle d^{\dagger}_{l,n}|\,\frac{\boldsymbol{\sigma}}{2}\,|d_{l,n}\rangle \\ &= \frac{1}{2}\,\langle c^{\dagger}_{l,n}\,(i\sigma_y)^n\boldsymbol{\sigma}(-i\sigma_y)^n\,c_{l,n}\rangle \\ &= \frac{1}{2}\,\mathrm{Tr}\,\rho(0)\,c^{\dagger}_{l,n}\,\sigma_y^n\boldsymbol{\sigma}\sigma_y^n\,c_{l,n} \\ &= \frac{1}{4}\,(\langle 0|\varphi_n^*\,c_{0,n,\uparrow}c^{\dagger}_{l,n}\sigma_y^n\boldsymbol{\sigma}\sigma_y^n\,c_{l,n}\,\varphi_n\,c^{\dagger}_{0,n,\uparrow}|0\rangle \\ &\qquad +\langle 0|\varphi_n^*\,c_{0,n,\downarrow}c^{\dagger}_{l,n}\sigma_y^n\boldsymbol{\sigma}\sigma_y^n\,c_{l,n}\,\varphi_n\,c^{\dagger}_{0,n,\downarrow}|0\rangle), \end{aligned} \tag{A5}$$

where $\boldsymbol{\sigma}$ is the vector of Pauli matrices, $\varphi_n$ is the spatial wave function of the initial polaron, which is the same for both spin states, and we use the convention that the central chain has index $l = 0$. From this, we obtain

$$\begin{aligned} &\langle d^{\dagger}_{l,n}|\,\frac{\boldsymbol{\sigma}}{2}\,|d_{l,n}\rangle \\ &= \frac{1}{4}\,|\varphi_n|^2\,\delta_{l,0}\big[\big(\sigma_y^n\boldsymbol{\sigma}\sigma_y^n\big)_{\uparrow\uparrow} + \big(\sigma_y^n\boldsymbol{\sigma}\sigma_y^n\big)_{\downarrow\downarrow}\big] \\ &= \frac{1}{4}\,|\varphi_n|^2\,\delta_{l,0}\,\mathrm{Tr}\,\sigma_y^n\boldsymbol{\sigma}\sigma_y^n \\ &= \frac{1}{4}\,|\varphi_n|^2\,\delta_{l,0}\,\mathrm{Tr}\,\boldsymbol{\sigma} = 0. \end{aligned} \tag{A6}$$

Hence, the initial state has full SU(2) symmetry also with respect to the spin of the new fermions. Together with the U(1) invariance of the Hamiltonian, this implies that, at all times, the new fermions can only develop a polarization in the $x$ direction.

We are not quite finished yet since the spin of the physical $c$ fermions is related to the spin of the $d$ fermions by spin rotations about the $y$ axis. Hence, an allowed $d$-spin polarization along the $x$ direction might generate a $c$-spin polarization along the $z$ direction, which would falsify our proposition. However, the transformation in Eqs. (A2) and (A3) only involves rotations about the $y$ axis by multiples of $\pi$ since $i\sigma_y = \exp[i(\sigma_y/2)\pi]$. This inverts the $x$ component of the spin for odd-$n$ sites but cannot lead to a polarization along $z$. In conclusion, for $t^{l}_{n,n+1} = 0$, we also obtain $\langle S_{z,l}\rangle(t) = 0$.

*Case 4*: $t^{\perp} = 0$. We introduce new fermionic operators

$$d_{l,n} = (-i\sigma_x)^l\, c_{l,n}, \qquad d^{\dagger}_{l,n} = c^{\dagger}_{l,n}\,(i\sigma_x)^l, \tag{A7}$$

from which

$$c_{l,n} = (i\sigma_x)^l\, d_{l,n}, \qquad c^{\dagger}_{l,n} = d^{\dagger}_{l,n}\,(-i\sigma_x)^l. \tag{A8}$$

There are two changes compared with the previous case: $\sigma_x$ replaces $\sigma_y$, and the spin-rotation factor winds in the $l$ direction instead of the $n$ direction. The Hamiltonian reads as

$$\begin{aligned} H = &-\sum_{l,n}t^{l}_{n,n+1}[\exp(-i\gamma A)d^{\dagger}_{l,n+1}d_{l,n} + \text{H.c.}] \\ &+t_{\rm so}\sum_{l,n}(-1)^l[\exp(-i\gamma A)d^{\dagger}_{l,n+1}i\sigma_y d_{l,n} + \text{H.c.}] \\ &+t^{\perp}_{\rm so}\sum_{l,n}(d^{\dagger}_{l+1,n}d_{l,n} + \text{H.c.}), \end{aligned} \tag{A9}$$

which now only contains $\sigma_y$. The argument is then analogous to the previous case.

To conclude, whenever one of the terms in the Hamiltonian $H_e$ is zero, a U(1) symmetry prevents the generation of a nonzero spin polarization along $z$ out of an unpolarized initial mixed state.


[1] M. I. Dyakonov and V. I. Perel, JETP Lett. **13**, 467 (1971).
[2] M. I. Dyakonov and V. I. Perel, Phys. Lett. A **35**, 459 (1971).
[3] J. E. Hirsch, Phys. Rev. Lett. **83**, 1834 (1999).
[4] J. Sinova, D. Culcer, Q. Niu, N. A. Sinitsyn, T. Jungwirth, and A. H. MacDonald, Phys. Rev. Lett. **92**, 126603 (2004).
[5] J. Sinova, S. O. Valenzuela, J. Wunderlich, C. H. Back, and T. Jungwirth, Rev. Mod. Phys. **87**, 1213 (2015).
[6] T. Kimura, Y. Otani, T. Sato, S. Takahashi, and S. Maekawa, Phys. Rev. Lett. **98**, 156601 (2007).
[7] E. Saitoh, M. Ueda, H. Miyajima, and G. Tatara, Appl. Phys. Lett. **88**, 182509 (2006).
[8] K. Ando and E. Saitoh, Nat. Commun. **3**, 629 (2012).
[9] D. Wei, M. Obstbaum, M. Ribow, C. H. Back, and G. Woltersdorf, Nat. Commun. **5**, 3768 (2014).
[10] S. O. Valenzuela and M. Tinkham, Nature (London) **442**, 176 (2006).
[11] Y. K. Kato, R. C. Myers, A. C. Gossard, and D. D. Awschalom, Science **306**, 1910 (2004).
[12] J. Wunderlich, B. Kaestner, J. Sinova, and T. Jungwirth, Phys. Rev. Lett. **94**, 047204 (2005).
[13] W. J. M. Naber, S. Faez, and W. G. van der Wiel, J. Phys. D: Appl. Phys. **40**, R205 (2007).

[14] V. A. Dediu, L. E. Hueso, I. Bergenti, and C. Taliani, Nat. Mater. **8**, 707 (2009).
[15] T. Sugawara and M. M. Matsushita, J. Mater. Chem. **19**, 1738 (2009).
[16] L. Nuccio, M. Willis, L. Schulz, S. Fratini, F. Messina, M. D'Amico, F. L. Pratt, J. S. Lord, I. McKenzie, M. Loth *et al.*, Phys. Rev. Lett. **110**, 216602 (2013).
[17] S. Bandyopadhyay, Phys. Rev. B **81**, 153202 (2010).
[18] Z. Liu, Z. F. Wang, J. W. Mei, Y. S. Wu, and F. Liu, Phys. Rev. Lett. **110**, 106804 (2013).
[19] Z. F. Wang, N. H. Su, and F. Liu, Nano Lett. **13**, 2842 (2013).
[20] S. Schott, E. R. McNellis, C. B. Nielsen, H. Y. Chen, S. Watanabe, H. Tanaka, I. McCulloch, K. Takimiya, J. Sinova, and H. Sirringhaus, Nat. Commun. **8**, 15200 (2017).
[21] E. R. McNellis, S. Schott, H. Sirringhaus, and J. Sinova, Phys. Rev. Mater. **2**, 074405 (2018).
[22] Z. G. Yu, Phys. Rev. Lett. **106**, 106602 (2011).
[23] Z. G. Yu, Phys. Rev. B **85**, 115201 (2012).
[24] K. Ando, S. Watanabe, S. Mooser, E. Saitoh, and H. Sirringhaus, Nat. Mater. **12**, 622 (2013).
[25] D. Sun, K. J. van Schooten, M. Kavand, H. Malissa, C. Zhang, M. Groesbeck, C. Boehme, and Z. V. Vardeny, Nat. Mater. **15**, 863 (2016).
[26] P. Wang, L. F. Zhou, S. W. Jiang, Z. Z. Luan, D. J. Shu, H. F. Ding, and D. Wu, Phys. Rev. Lett. **120**, 047201 (2018).
[27] M. M. Qaid, M. R. Mahani, J. Sinova, and G. Schmidt, Phys. Rev. Res. **2**, 013207 (2020).
[28] Z. G. Yu, Phys. Rev. Lett. **115**, 026601 (2015).
[29] U. Chopra, S. A. Egorov, J. Sinova, and E. R. McNellis, J. Phys. Chem. C **123**, 19112 (2019).
[30] M. R. Mahani, U. Chopra, and J. Sinova, arXiv:2002.11092.
[31] S. Watanabe, K. Ando, K. Kang, S. Mooser, Y. Vaynzof, H. Kurebayashi, E. Saitoh, and H. Sirringhaus, Nat. Phys. **10**, 308 (2014).
[32] W. P. Su, J. R. Schrieffer, and A. J. Heeger, Phys. Rev. Lett. **42**, 1698 (1979).
[33] D. Obana, F. Liu, and K. Wakabayashi, Phys. Rev. B **100**, 075437 (2019).
[34] A. Mukherjee, A. Nandy, S. Sil, and A. Chakrabarti, Phys. Rev. B **105**, 035428 (2022).
[35] F. Mireles and G. Kirczenow, Phys. Rev. B **64**, 024426 (2001).
[36] R. E. Peierls, *Quantum Theory of Solids* (Clarendon Press, Oxford, 1955).
[37] A. J. Heeger, S. Kivelson, J. R. Schrieffer, and W. P. Su, Rev. Mod. Phys. **60**, 781 (1988).
[38] Y. Ono and A. Terai, J. Phys. Soc. Jpn. **59**, 2893 (1990).
[39] J. Lei, H. Li, S. Yin, and S. J. Xie, J. Phys.: Condens. Matter **20**, 095201 (2008).
[40] R. W. Brankin, I. Gladwell, and L. F. Shampine, RKSUITE: Software for ODE IVPS, http://www.netlib.org.
[41] A. A. Johansson and S. Stafström, Phys. Rev. B **69**, 235205 (2004).
[42] X. J. Liu, K. Gao, J. Y. Fu, Y. Li, J. H. Wei, and S. J. Xie, Phys. Rev. B **74**, 172301 (2006).
[43] Y. Y. Miao, H. J. Kan, D. Li, C. K. Wang, J. F. Ren, and G. C. Hu, Phys. Lett. A **433**, 128024 (2022).
[44] O. Entin-Wohlman, A. Aharony, Y. M. Galperin, V. I. Kozub, and V. Vinokur, Phys. Rev. Lett. **95**, 086603 (2005).
[45] We have convinced ourselves that the small result is not a numerical artifact by setting each of the parameters $t^{\perp}$, $t_{\rm so}$, and $t_{\rm so}^{\perp}$ to zero in turn (not shown). This causes the SHE to vanish, as above, which for the numerics means that the resulting numbers are on the order of machine precision.
[46] H. F. Meng and C. M. Lai, Phys. Rev. B **55**, 13611 (1997).